Calibration of a neutron time-of-flight detector with a rapid instrument response function for measurements of bulk fluid motion on OMEGA

O. M. Mannion, V. Yu. Glebov, C. J. Forrest, J. P. Knauer, V. N. Goncharov, S. P. Regan, T. C. Sangster, C. Stoeckl, and M. Gatu Johnson

Citation: Review of Scientific Instruments **89**, 10I131 (2018); doi: 10.1063/1.5037324
View online: https://doi.org/10.1063/1.5037324
View Table of Contents: http://aip.scitation.org/toc/rsi/89/10
Published by the American Institute of Physics

Calibration of a neutron time-of-flight detector with a rapid instrument response function for measurements of bulk fluid motion on OMEGA

O. M. Mannion,[1,a)] V. Yu. Glebov,[1] C. J. Forrest,[1] J. P. Knauer,[1] V. N. Goncharov,[1] S. P. Regan,[1] T. C. Sangster,[1] C. Stoeckl,[1] and M. Gatu Johnson[2]
[1]*Laboratory or Laser Energetics, University of Rochester, Rochester, New York 14623, USA*
[2]*Massachusetts Institute of Technology, Plasma Science and Fusion Center, Cambridge, Massachusetts 02139, USA*

(Presented 16 April 2018; received 23 April 2018; accepted 3 July 2018; published online 11 October 2018)

A newly developed neutron time-of-flight (nTOF) diagnostic with a fast instrument response function has been fielded on the OMEGA laser in a highly collimated line of sight. By using a small plastic scintillator volume, the detector provides a narrow instrument response of 1.7 ns full width at half maximum while maintaining a large signal-to-noise ratio for neutron yields between 10^{10} and 10^{14}. The OMEGA hardware timing system is used along with an optical fiducial to provide an absolute nTOF measurement to an accuracy of ~56 ps. The fast instrument response enables the accurate measurement of the primary deuterium-tritium neutron peak shape, while the optical fiducial allows for an absolute neutron energy measurement. The new detector measures the neutron mean energy with an uncertainty of ~7 keV, corresponding to a hot-spot velocity projection uncertainty of ~12 km/s. Evidence of bulk fluid motion in cryogenic targets is presented with measurements of the neutron energy spectrum. *Published by AIP Publishing.* https://doi.org/10.1063/1.5037324

I. INTRODUCTION

In inertial confinement fusion (ICF) experiments performed on OMEGA, a spherical shell of deuterium-tritium (DT) ice or CH plastic is filled with DT gas. A laser illuminates the shell applying an ablative pressure which accelerates the shell radially inward. As the shell converges, it compresses the DT gas, converting its kinetic energy into thermal energy of the gas. This spherical compression produces a hot spot at temperatures and densities that allow fusion reactions to occur.

To achieve maximum conversion of a shell's kinetic energy to hot-spot thermal energy, a spherically symmetric implosion is desired. In reality, implosions suffer from both low-mode[1] and high-mode[2] asymmetries, which degrade implosion performance. Understanding and measuring the degradation in performance caused by real-world asymmetries is vital to optimize direct-drive implosions and constrain theoretical models.

Bulk collective motion of the hot spot is characteristic of implosions with low-mode asymmetries.[3,4] Measurements of bulk collective motion in ICF experiments would confirm the existence of low-mode asymmetries and give indications of the perturbation strength. This work describes a method to measure bulk collective motion of the hot spot in ICF experiments by measuring the primary DT fusion neutron energy spectrum.

The neutron energy spectrum produced by a stationary fusing fluid element was studied non-relativistically by Brysk[5] and semi-relativistically by Ballabio.[6] The neutron energy spectrum produced by a moving fusing fluid element was studied fully relativistically by Appelbe[7,8] and Munro.[9,10] These results showed that the shape of the neutron energy spectrum is approximately Gaussian with moments that depend not only on the plasma ion temperature but also on the fluid element velocity. In particular, if the fluid element is moving with a bulk collective motion, the first moment of the neutron energy spectrum is shifted depending on the magnitude of the projection of the fluid velocity along the measurement axis.

The relationship between the fluid element velocity and the corresponding neutron energy shift has been derived non-relativistically by Murphy[11] and relativistically by Zylstra.[12] Assuming all bulk collective motion is along the line of sight (LOS) of the measurement, the relativistic relationship can be written as

$$\beta_f = \frac{\beta - \beta_0}{1 - \beta\beta_0}, \tag{1}$$

where β_f is the fluid element bulk flow velocity in the lab frame, β is the measured neutron velocity in the lab frame, and β_0 is the neutron velocity in the fluid element frame, each normalized to the speed of light. The neutron velocity is related to the mass normalized neutron energy $\chi = \frac{E}{m_n}$ by

$$\beta = \frac{\sqrt{\chi^2 + 2\chi}}{\chi + 1}. \tag{2}$$

By using Eqs. (1) and (2), shifts in the neutron energy spectrum can be interpreted as bulk collective motion of the fusing fluid element.

In ICF experiments, there is not just a single fusing fluid element; instead there is a collection of fusing fluid elements within the hot spot that are distributed in space and time. Since measurements of the neutron energy spectrum are

Note: Paper published as part of the Proceedings of the 22nd Topical Conference on High-Temperature Plasma Diagnostics, San Diego, California, April 2018.

a)omann@lle.rochester.edu

both spatially and temporally integrated, we interpret shifts in the first moment of the neutron energy spectrum as the neutron-averaged hot-spot bulk collective fluid velocity.

Simulations of cryogenic OMEGA implosions with low-mode asymmetries caused by real-world effects such as laser illumination nonuniformity, target offset, and ice roughness showed neutron-averaged hot-spot bulk collective motion as large as 100 km/s along particular measurement axes.[4] Previous measurements of shifts in the first moment of the neutron energy spectrum inferred bulk collective motion of the hot spot as large as 210 ± 30 km/s in polar-direct-drive (PDD) experiments at the National Ignition Facility (NIF) using the magnetic recoil spectrometer.[13] Measurements in direct-drive experiments on OMEGA with a CR-39-based recoil spectrometer[12] with a velocity resolution of ~50–75 km/s lacked the resolution required to measure fluid velocities relevant on OMEGA.

In this paper, we present measurements of shifts in the first moment of the neutron energy spectrum using the neutron time-of-flight (nTOF) technique.[14] In Sec. II, we describe a new nTOF detector fielded on OMEGA that is used to measure bulk collective motion of the hot spot. Section III describes the detector calibration including measurements of the detector instrument response function (IRF) and the absolute timing calibration. In Sec. IV, we report measurements of bulk collective motion in cryogenic implosions. Finally, Sec. V presents conclusions and discusses an extension of this method to four lines of sight.

II. DETECTOR DESIGN

The neutron energy spectrum produced in OMEGA implosions is measured using a series of nTOF spectrometers.[15] Recent increases in neutron yields greater than 10^{14} on OMEGA have provided high neutron statistics for the nTOF detectors.[16]

A new nTOF detector has been built to take advantage of the increased neutron yield. By decreasing the scintillator volume, the new detector provides a fast IRF of 1.7-ns full width at half maximum (FWHM) while maintaining a large signal-to-noise ratio for neutron yields between 10^{10} and 10^{14}. The detector response is considered fast relative to the nTOF spectrum FWHM which, for this detector location, is greater than 2 ns at nominal OMEGA plasmas temperatures greater than 2 keV. A fast instrument response minimizes the distortion of the incoming primary DT neutron signal by the detector IRF and therefore enables accurate measurements of primary DT neutron energy spectrum.

The new detector consists of a 50-mm × 50-mm × 5-mm quenched plastic scintillator [EJ-232Q-1% (BC-422Q)],[17] attached to a 15-cm acrylic light guide, which is coupled to a Photek 140 photomultiplier tube (PMT).[18] The PMT is operated at a constant bias of −4.7 kV to ensure a stable PMT response and sufficient gain. The PMT signal is transported to a four-channel 10-GSamples/s Tektronix oscilloscope by a 5-m LMR-400 coaxial cable. To maximize light-collection efficiency, the entire scintillator and light-guide connection is covered in a light-tight wrapping. The detector design is shown in Fig. 1.

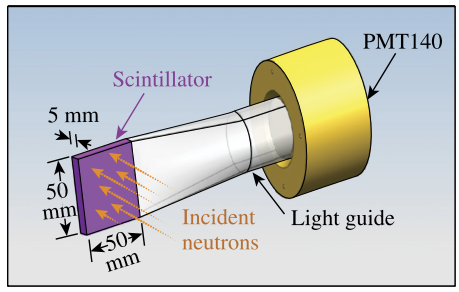

FIG. 1. The detector design consists of small quenched plastic scintillator (purple) connected to a light guide, which is connected to a photomultiplier tube (PMT140) (yellow). Neutrons (orange) are incident on the front face of the scintillator.

The detector is located in a well-collimated LOS 13.0 m from target chamber center (TCC) in the southern hemisphere of the OMEGA target chamber along the P7 port. This is the only shielded LOS on OMEGA and allows for all relevant electronics, including the PMT, to be out of the LOS of the primary neutron beam while also minimizing the signal from neutrons scattering off the OMEGA target chamber. The combination of these two features results in an extremely high quality signal.

III. DETECTOR CALIBRATION

A. Instrument response function

The IRF can be constructed by considering the detector's neutron and photon responses. The neutron response measures the neutron transit time through the detector, while the photon response measures the recorded electronic signal as a function of time for an impulse photon signal. The actual IRF is a convolution of these two components.[19]

As a result of the thin scintillator design, the transit time of a 14-MeV neutron through the scintillator is ~100 ps. Additionally, the thin scintillator design ensures that less than 1% of the incident neutrons will undergo multiple scattering within the scintillator volume. Both of these considerations result in the neutron response being well approximated by a delta function in time. For this reason, the IRF for this detector is simply the photon response.

The detector photon response, and therefore the detector IRF, has been measured *in situ* by recording the detector response to x-ray impulse signals created by illuminating a Au sphere or Au foil with a 20- or 100-ps-long Gaussian laser pulse. The x-ray signal produced in these experiments had a temporal width between 70 and 100 ps as measured by the neutron temporal diagnostic (NTD).[20] The x-ray signals produced in these experiments therefore approximate a delta function in time incident on our detector, and so the recorded signal is a direct measurement of the IRF.

The detector IRF was measured over a six-month period with ten x-ray calibration shots of varying x-ray intensities. The IRF was found to be extremely stable over this period with no deviations observed. An average IRF was constructed by normalizing and aligning the measured signals to their peak and is shown in Fig. 2 along with the ten measured signals.

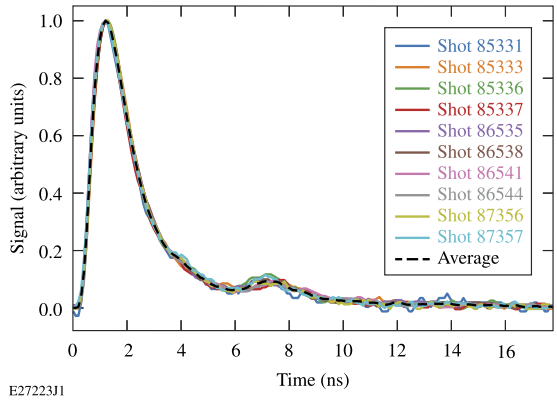

FIG. 2. The measured x-ray signals from a series of calibration experiments along with the averaged shape. All signal peaks have been aligned in time and normalized. The FWHM of this detector IRF is 1.7 ns with a rise time (10%–90%) of 0.6 ns. The bump ~5 ns after the main peak is attributed to scattering within the OMEGA Laser Facility.

The exponentially modified Gaussian shape of the IRF is characteristic of scintillator detectors, which have a finite excitation lifetime. The average detector IRF has a measured FWHM of 1.7 ns with a rise time (10%–90%) of 0.6 ns. The bump ~5 ns after the main peak is a unique feature of this detector configuration and is attributed to scattering within the OMEGA Laser Facility. Future work will focus on eliminating this background source.

B. Absolute timing calibration

To measure the absolute time of flight (TOF) of a signal, the recorded time axis must be calibrated and aligned such that the origin is the moment the signal is produced at TCC. Additionally a calibration is required to eliminate any inherent delay and mistiming in the detector with respect to the OMEGA hardware timing system.

To properly time the recorded neutron or x-ray signal to the experiment, measurements of the laser pulse and neutron/x-ray bang times are required. Timing of the laser pulse at TCC is achieved with the p510 streak camera, which measures the laser pulse as it enters the target chamber.[21] The neutron/x-ray bang times are recorded with the NTD.[20] Each of these times are measured relative to the OMEGA timing fiducial. By injecting the same timing fiducial into the recorded neutron or x-ray signal, these measured quantities can be used to properly align the recorded signal with the experiment.

The transformation from a recorded signal time τ, which has an arbitrary timing origin, to the true TOF of the signal t, which is timed to the experiment, is given by

$$t = \tau - (\tau_0 + \Delta t_{\text{laser}} + \Delta t_{\text{bang}}) - \Delta t_{\text{cal}} - \Delta t_{\text{att}}, \qquad (3)$$

where τ_0 is the time of the measured fiducial on the recorded signal, Δt_{laser} is the delay between the start of the laser pulse (defined as 2% of the maximum laser power) and the fiducial as reported by the p510 streak camera, Δt_{bang} is the delay between the neutron/x-ray bang time and the beginning of the laser pulse as reported by the NTD, Δt_{cal} is a calibration constant accounting for any inherent delays and mistiming in our detector device, and Δt_{att} accounts for additional delays in the signal timing if a signal attenuator is used.

To determine Δt_{cal}, a particle i with a known TOF t_i is recorded and the measured TOF τ_i is determined. Asserting that the known TOF is t_i, Eq. (3) can be solved for Δt_{cal} by using the measured laser pulse and bang time. X-ray signals are ideal for timing-calibration experiments because the TOF is uniquely determined by the detector distance. The x-ray signals used to construct the IRF are used for this timing calibration.

The most accurate method to measure τ_x, the uncalibrated x-ray TOF, is a template-fitting algorithm.[22,23] This method relies on fitting a scaled and translated version of a template signal to the measured data. The main advantage of this technique is that there is no ambiguity in the starting time of the signal, and all timing delays are included in the template function used for the fit.

In our application, the template signal $m(t)$ is the averaged IRF shown in Fig. 2. The actual fitting function is given by

$$g(\tau; A, \tau_x) = A \;\; m(\tau - \tau_x)\,. \qquad (4)$$

In practice, $m(t)$ is a cubic spline interpolation of the template function. Once this function is constructed, a least squares fit can be performed on a measured x-ray pulse to determine A and τ_x. An example of this fit is shown for shot 87356 in Fig. 3.

The template-fitting algorithm has been applied to determine τ_x and therefore Δt_{cal} for the eight x-ray calibration shots in Sec. III A that had a timing fiducial. Figure 4 shows the inferred calibration constant for each shot. The average calibration constant from these shots was determined to be $\Delta t_{\text{cal}} = 18.840 \pm 0.015$ ns. The ~44-ps uncertainty in each measurement of Δt_{cal} was determined from the standard deviation of all eight measurements.

The uncertainties in the measured nTOF was determined by considering the statistical and systematic uncertainties. There is a statistical uncertainty associated with any fit in the recorded signal time τ of ~5 ps as well as in the fiducial signal time τ_0 of ~3 ps. The statistical uncertainty for the terms Δt_{laser} and Δt_{bang} are ~5 ps and ~10 ps, respectively. The statistical uncertainty in the term Δt_{att} has been measured to be ~1 ps. There is a systematic uncertainty in Δt_{bang} of ~40 ps as well as the ~15 ps in Δt_{cal} determined above. Adding

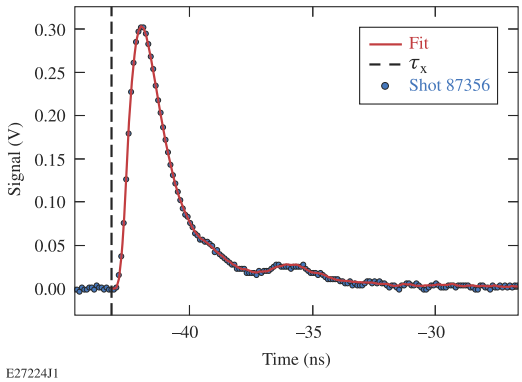

FIG. 3. Template fit for x-ray shot 87356 to determine τ_x. The best-fit values are $A = 0.303 \pm 0.001$ V and $\tau_x = -43.162 \pm 0.002$ ns. Note that the fit is performed in the uncalibrated time axis of the oscilloscope, so the absolute value of the time holds no significance.

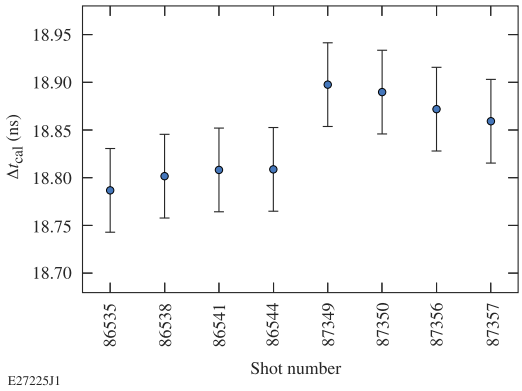

FIG. 4. The measured calibration constant for the eight x-ray calibration shots with a timing fiducial, each with an uncertainty of ~44 ps. The average calibration constant was determined to be $\Delta t_{cal} = 18.840 \pm 0.015$ ns.

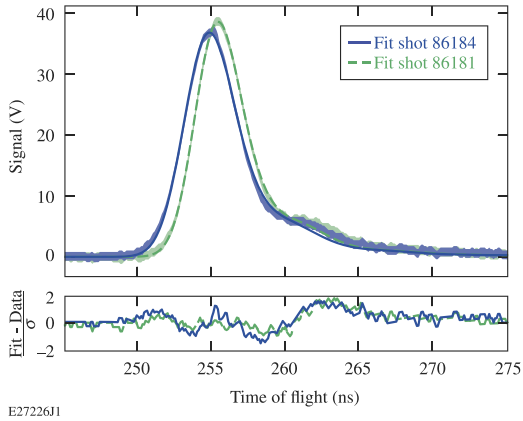

FIG. 5. The measured nTOF signal bounded by signal noise ±1 σ (shaded) with the corresponding forward fit (solid line) for two consecutive cryogenic shots 86181 and 86184. The TOF shift corresponds to a difference in fluid velocity projections of ~125 km/s.

the statistical and systematic uncertainties in quadrature separately gives a total systematic uncertainty of ~43 ps and a total statistical uncertainty of ~13 ps. Adding the systematic and statistical uncertainties, we find a total timing uncertainty of ~56 ps. This timing uncertainty corresponds to a total neutron energy uncertainty of ~7 keV and a bulk collective velocity uncertainty of ~12 km/s.

If the inferred ion temperature from the neutron energy spectrum is inflated because of nonthermal components to the second central moment associated with fluid motion,[7,11] the thermal component to the first moment[6] will also be inflated. Since the inferred ion temperature is always greater than or equal to the thermal temperature,[11] and the thermal component to the first moment is a monotonically increasing function of ion temperature,[6] a larger thermal component to the first moment is always predicted. To compensate for this, a bulk collective motion away from the detector will be inferred. This effect has been estimated with Monte Carlo calculations, and it was found that a 0.75-keV overprediction of the thermal temperature would lead to a systematic error in the bulk collective velocity of at most −6 km/s.

IV. MEASUREMENTS

The nTOF signal for a series of nominal cryogenic and room-temperature experiments has been measured, and the time axes have been calibrated using Eq. (3). To determine the moments of the neutron energy spectrum, the forward-fit method[19] was applied using the averaged IRF measured in Sec. III A. Shifts in the mean neutron energy were then interpreted as bulk collective fluid motion with the use of Eqs. (1) and (2).

Example nTOF traces for two consecutive cryogenic targets are shown in Fig. 5. The timing difference between these signals resulting from flows was ~60 ps and corresponds to a mean neutron energy difference of ~68 keV and a fluid velocity projection difference of ~125 km/s. The measured neutron yield and minimum measured DT ion temperature were 1.01×10^{14} and 3.9 keV for shot 86181 and 1.06×10^{14} and 4.5 keV for shot 86184. The target offset for shot 86181 was −32 μm along the OMEGA P7 direction. When a large target offset exists, the laser intensity on target is asymmetric,[24] which can lead to a bulk collective motion of the capsule and may be the source of the large flow projection observed for shot 86181.

Figure 6 shows inferred hot-spot fluid velocity projection along the measurement axis for each experiment. Large variations in the inferred flow velocity projections are observed in cryogenic experiments but not in room-temperature implosions, indicating residual motion of the hot spot at peak neutron production may exist for cryogenic implosions. Additionally cryogenic experiments show a systematic projected flow of 42 km/s along the OMEGA P7 axis, while the average projected flow for room-temperature experiments is −6 km/s. The systematic projected flow in cryogenic experiments is hypothesized to be caused by either a systematic ice nonuniformity or the stalk and will be the focus of future work.

Measurements of the hot-spot velocity projection inferred from this detector will be used in the future to test the validity of radiation-hydrodynamic codes. Additionally, insights into the residual kinetic energy contained within the hot spot will

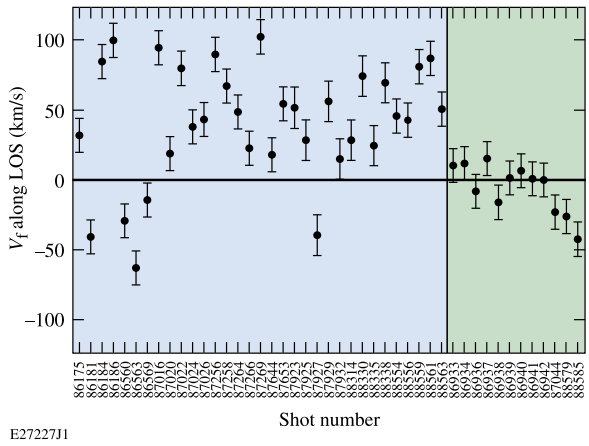

FIG. 6. The inferred bulk collective velocity along the detector LOS for a series of cryogenic implosions (blue) and room-temperature implosions (green). There are significant variations in the inferred flows along the detector LOS in cryogenic targets, indicating residual motion of the hot spot. Additionally a systematic flow toward the P7 port is observed for cryogenic experiments.

be found by combining measured bulk flows with the inferred ion temperature variations.

V. CONCLUSION

A new nTOF detector capable of measuring the absolute neutron energy spectrum has been fielded on the OMEGA laser. The detector IRF has been measured *in situ* and has been calibrated with x-ray timing experiments. A method has been described to infer bulk fluid velocity of the neutron-producing region in ICF experiments; measurements of this motion in cryogenic targets show velocities as large as 103 ± 12 km/s.

Future work will extend this analysis to multiple lines of sight to determine the complete bulk fluid velocity vector. Extending this measurement to three LOS would allow for the determination of the three components of the bulk fluid velocity vector. With four measurements of the neutron mean energy, each component of the bulk collective velocity could be determined in addition to the thermal temperature without relying on measurements of the second moment. This would eliminate the systematic uncertainty associated with the nonthermal component of the second moment discussed in Sec. III B, which leads to a decrease in the inferred flows.

ACKNOWLEDGMENTS

This material is based on the work supported by the Department of Energy National Nuclear Security Administration under Award No. DE-NA0001944, the University of Rochester and the New York State Energy Research and Development Authority.

[1]R. C. Shah *et al.*, Phys. Rev. Lett. **118**, 135001 (2017).
[2]P. B. Radha *et al.*, Phys. Plasmas **12**, 056307 (2005).
[3]B. K. Spears *et al.*, Phys. Plasmas **21**, 042702 (2014).
[4]I. V. Igumenshchev *et al.*, Phys. Plasmas **24**, 056307 (2017).
[5]H. Brysk, Plasma Phys. **15**, 611 (1973).
[6]L. Ballabio, J. Källne, and G. Gorini, Nucl. Fusion **38**, 1723 (1998).
[7]B. Appelbe and J. Chittenden, Plasma Phys. Controlled Fusion **53**, 045002 (2011).
[8]B. Appelbe and J. Chittenden, High Energy Density Phys. **11**, 30 (2014).
[9]D. H. Munro, Nucl. Fusion **56**, 036001 (2016).
[10]D. H. Munro, J. E. Field, R. Hatarik, J. L. Peterson, E. P. Hartouni, B. K. Spears, and J. D. Kilkenny, Phys. Plasmas **24**, 056301 (2017).
[11]T. J. Murphy, Phys. Plasmas **21**, 072701 (2014).
[12]A. B. Zylstra *et al.*, Rev. Sci. Instrum. **85**, 063502 (2014).
[13]M. G. Johnson *et al.*, Phys. Plasmas **20**, 042707 (2013).
[14]R. A. Lerche, L. W. Coleman, J. W. Houghton, D. R. Speck, and E. K. Storm, Appl. Phys. Lett. **31**, 645 (1977).
[15]V. Y. Glebov, presented at the nTOF Diagnostic Workshop at Lawrence Livermore National Laboratory, Livermore, CA, 18 July 2017.
[16]V. Gopalaswamy, Laboratory for Laser Energetics, private communication (2018).
[17]Eljen Technology, Sweetwater, TX 79556, USA.
[18]Photek Ltd., St. Leonards on Sea, East Sussex, TN38 9NS, United Kingdom.
[19]R. Hatarik *et al.*, J. Appl. Phys. **118**, 184502 (2015).
[20]C. Stoeckl *et al.*, Rev. Sci. Instrum. **87**, 053501 (2016).
[21]W. R. Donaldson, R. Boni, R. L. Keck, and P. A. Jaanimagi, Rev. Sci. Instrum. **73**, 2606 (2002).
[22]B. W. Adams, A. Elagin, H. J. Frisch, R. Obaid, E. Oberla, A. Vostrikov, R. G. Wagner, J. Wang, and M. Wetstein, Nucl. Instrum. Methods Phys. Res., Sect. A **795**, 1 (2015).
[23]W. E. Cleland and E. G. Stern, Nucl. Instrum. Methods Phys. Res., Sect. A **338**, 467 (1994).
[24]J. R. Rygg *et al.*, Phys. Plasmas **15**, 034505 (2008).